Electronic structure of monolayer graphite on a TiC(111) surface

Katsuyoshi Kobayashi and Masaru Tsukada
Department of Physics, Faculty of Science, University of Tokyo, Hongo 7-3-1, Bunkyo-ku, Tokyo 113, Japan
(Received 28 July 1993; revised manuscript received 11 November 1993)

The electronic structure of monolayer graphite on a TiC(111) surface is investigated by first-principles band calculations. Occupied π bands of the graphite layer are similar to those of bulk graphite with a constant shift to a lower-energy region. Unoccupied π^* bands are drastically deformed by hybridization with the substrate. The calculated band structure reproduces well an experimental band dispersion. Calculated electronic charges show no charge transfer from the substrate to the graphite layer. The lowering of the π bands is explained by a change of electronic occupation in the graphite layer from the occupied σ and π states to the unoccupied π^* states due to hybridization with the substrate. The calculated results are consistent with the observed anomalous expansion of the lattice constant of monolayer graphite on metal substrates. The calculated band dispersion and electronic charges do not depend on the lateral position of the monolayer graphite relative to the substrate, which is explained by an averaging effect in incommensurate systems. Scanning-tunneling-microscopy (STM) images calculated from the results of the band calculation do not show the atomic structure of the graphite but show superstructures, which explain the experimental STM images.

I. INTRODUCTION

Graphite is a prototype of layered materials, and has been studied extensively. The electronic structure of graphite shows highly anisotropic and unique properties. Graphite is commonly used also as a standard sample in scanning tunneling microscopy (STM) because of the flatness of its surface.[1] The STM image of the graphite surface shows a triangular-lattice pattern, which is different from what would be expected from its honeycomb atomic structure.[2] This result was considered rather strange at fist, but now has been explained by the fact that the STM images reflect not the atomic structure of the surface but the electronic structure near the Fermi level.[3]

Recently, phonon structures of monolayer graphite grown on various metal surfaces have been measured extensively, and interesting properties have been found.[4–8] Depending on the substrate, the phonon structure of the monolayer graphite differs or does not differ from that of bulk graphite. In the former case, the C-C bond strength in the graphite layer is much weaker than that of bulk graphite, and binding of the graphite layer to the substrate is stronger than the interlayer binding of bulk graphite.[4]

So far, the weakening of the C-C bond in monolayer graphite has been explained in terms of a rigid-band model with an electronic charge transfer from the substrate to the graphite layer.[4,9] The unoccupied π^* band of the graphite is partially filled with the transferred charge, which results in weakening of the C-C bond.

A similar phenomenon has been observed in graphite intercalation compounds (GIC's).[10] In GIC's, the charge transfer occurs between the graphite layer and the intercalant. The transferred charge weakens the C-C bond of graphite, and the graphite lattice expands. A first-principles electronic-structure calculation shows a relation between the amount of transferred charge and the expansion of the graphite lattice, which well reproduces the experimental results.[11] For monolayer graphite on TiC(111) surface, the charge transfer estimated from the relation for GIC's is 0.4 electrons per C atom, which is considerably larger than the charge transfer of the many donor GIC's. In other words, the lattice constant of monolayer graphite on metal surfaces is anomalously expanded.

Angle-resolved ultraviolet photoelectron spectroscopy (ARUPS) of monolayer graphite on the TiC(111) surface shows a distinct band dispersion, which is similar to the occupied π band structure of bulk graphite but shifted to a lower-energy region by a few eV.[12] The amount of charge transfer estimated from the ARUPS data assuming the rigid-band model is 0.02 electrons per C atom, which is much smaller than that estimated from the lattice-constant expansion as a result of the first-principles calculation. Moreover, the peaks of x-ray photoelectron spectra of monolayer graphite on the TiC(111) surface do not show a shift corresponding to charge transfer from the substrate to the graphite layer.[12]

Disagreement among the amounts of charge transfer estimated from several experiments shows that the electronic structure of monolayer graphite on metal surfaces cannot be explained by the simple rigid-band model with charge transfer. The small difference in the work function between the bulk graphite surface and the TiC(111) surface also does not support the charge-transfer mechanism.[12] Recent experiments with plasmon[13] and STM images[14,15] of monolayer graphite on metal surfaces also suggest that the influence of the substrate on the graphite layer is important.

The STM image of monolayer graphite on the TiC(111) surface shows a triangular-lattice pattern similar to that of pristine graphite.[14] The period of the pattern, however, is as long as 5 Å, which is different from that of bulk graphite. Furthermore, at certain bias voltages, a moiré pattern is observed, where the amplitude of the triangular pattern is modulated with a longer period of about 21 Å.

A low-energy electron-diffraction study has shown that the graphite layer is incommensurate with the substrate, and that the periods of the superstructure observed in the STM image correspond to multiple-scattering diffraction spots.[14] A moiré pattern has been observed in the STM images of monolayer graphite on other substrates, such as the Pt(111) surface.[15] Observation of superstructure in the STM image suggests that the electronic structure of monolayer graphite is locally modulated by the influence of the substrate.

The purpose of the present paper is to clarify theoretically the electronic structure of monolayer graphite on metal surfaces. For this purpose, first-principles band calculations are performed for monolayer graphite on a TiC(111) surface. The STM images are also calculated based on the results of the band calculations, to discuss the superstructures observed in experiments. In Sec. II, structural models and a method for calculation of the electronic structure and the STM image are given. Calculated results and discussions are presented in Sec. III, and our conclusion is stated in Sec. IV.

II. METHOD FOR CALCULATION OF THE ELECTRONIC STRUCTURE AND THE STM IMAGE

A. Structural model and method of band calculation

In performing an electronic-structure calculation of monolayer graphite on transition-metal surfaces, a difficulty arises from their incommensurate atomic structure except for the case of a Ni(111) substrate. In this paper, band calculations of monolayer graphite on the TiC(111) surface are performed by changing the lattice constant of the graphite layer slightly, so that the graphite layer becomes commensurate with the substrate. This change quantitatively influences such values as bandwidth, but it has been verified by performing the band calculation for several lattice constants that the results do not change qualitatively.

It has been determined experimentally that the lattice constants of the graphite layer and the TiC(111) surface are 2.50 and 3.06 Å, respectively, and the directions of their lattice vectors are rotated by 30° relative to each other.[14] Therefore, by expanding the lattice constant of the graphite layer by about 6%, the system becomes commensurate.

When an incommensurate substrate-overlayer system is rationally approximated by changing the lattice constant, the lateral position of the overlayer relative to the substrate is not well defined. In the study reported in this paper, the band calculations are performed for two cases with different lateral positions, and the dependence of the results obtained on the lateral position is investigated. Figure 1 shows the models of monolayer graphite on the TiC(111) surface used in this paper. The unit cell of the models corresponds to that of a 2×2 structure for the graphite layer and that of a $\sqrt{3}\times\sqrt{3}$ structure for the TiC(111) surface. The lattice constant of the unit cell is set at 5.30 Å.

In the band calculation, a slab model is used. The slab consists of one graphite layer and four TiC(111) layers. The unit cell contains 14 carbon atoms and six Ti atoms. Interlayer distances in the TiC(111) surface are taken to be the same as those in the bulk crystal. The height of the graphite layer measured from the top layer of the TiC(111) surface has not been determined experimentally. In this paper, the band calculation is performed for two heights, and the plausible height is determined by comparison with the experimental data. The selected height is (a) 2.16 and (b) 3.42 Å. The height in case (a) is the same as the C-Ti bond length in bulk TiC; the second case (b) is determined from an experimental value for monolayer graphite on the Ni(111) surface, taking into account the difference in atomic radius between Ti and Ni.[16] This value is almost the same as the interlayer distance in bulk graphite.

The band calculation is performed by the discrete variational $X\alpha$ method.[17–19] This is a first-principles method of electronic-structure calculation with localized orbital bases. The method is based on density-functional formalism with the local-density approximation.[20,21] The band calculation is performed with all electrons. Atomic basis orbitals from $1s$ up to $2s,2p$ for the C atom and up to $3d,4s,4p$ for the Ti atom are used. Self-consistency is checked by atomic-orbital charges calculated by Mullik-

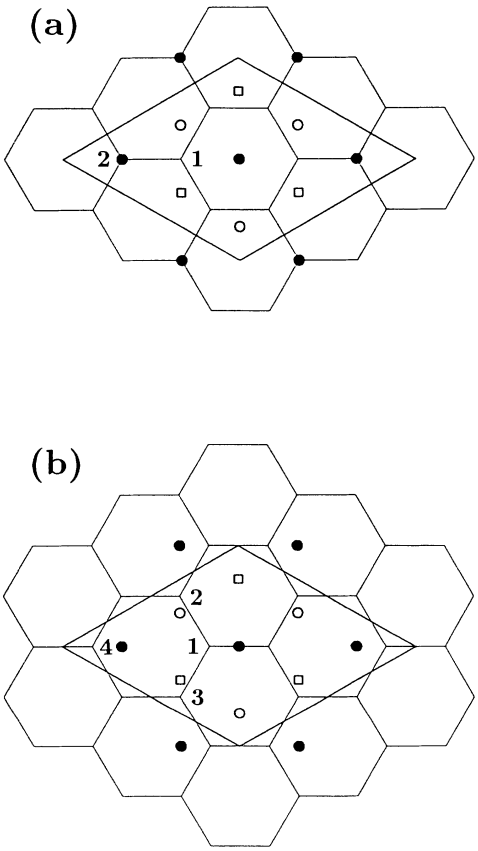

FIG. 1. Structural models for monolayer graphite on the TiC(111) surface: (a) Model A and (b) model B. The graphite lattice is shown by the honeycomb structure. Closed circles indicate first-layer Ti atoms and fourth-layer C atoms of the TiC(111) surface. Open circles and open squares indicate second-layer C atoms and third-layer Ti atoms, respectively. The rhombus shows the unit cell. The numbers in the figure distinguish the inequivalent C atoms in the graphite layer.

en population analysis.[22] The criterion for self-consistency is that all inconsistencies between input and output atomic-orbital charges are less than 0.01 electrons.

B. Method of calculation for the STM image

A simple method for calculating the tunneling current in the STM is the use of Tersoff and Hamann's formula[23] and its extension expressed as

$$I(V) \propto \int_{E_F}^{E_F+eV} dE\rho(\mathbf{r}_0,E) , \quad (1)$$

$$\rho(\mathbf{r},E) \equiv \sum_i |\Psi_i(\mathbf{r})|^2 \delta(E-E_i) . \quad (2)$$

In the above, $\rho(\mathbf{r},E)$, $\Psi_i(\mathbf{r})$, and E_F are the local density of states (LDOS) of the surface, the surface wave function with energy E_i, and the Fermi energy, respectively. This method allows us to obtain STM images from only the LDOS of the sample surface. In this study, the STM image is calculated by the above formula, since the effect of the tip is not responsible for the occurrence of the superstructures observed in STM images of monolayer graphite on metal substrates.

III. CALCULATED RESULTS AND DISCUSSION

A. Band structure and electronic charge

Figure 2 shows a calculated band structure of monolayer graphite on the TiC(111) surface. The calculation is performed for model A in Fig. 1. The graphite-substrate distance is taken as 2.16 Å. In this figure, two types of bands are seen. Many bands are concentrated near the Fermi level without significant dispersion. These are mainly the $3d$ bands of Ti. Below these bands, several bands are seen with relatively large dispersion. These are the σ bands of graphite. The π bands of graphite are mixed with the bands of the substrate, and it is difficult to distinguish them.

To clarify the π band structure of the graphite, bands with a comparatively large π-orbital component are selected. These bands, whose graphite $2p_z$ component is larger than 25%, are represented by heavy solid lines in Fig. 3. From the figure, distinct band dispersions are identified. The occupied π bands in an energy region from -10 eV to the Fermi level correspond well to those of bulk graphite projected onto the 2×2 unit cell. It is known that the Fermi level of bulk graphite is located at the K point in the unfolded Brillouin zone.[24] The K point in the unfolded Brillouin zone is folded to a K point in the Brillouin zone of the 2×2 unit cell, as indicated by the arrow in Fig. 3. The energy at about 2.5 eV below the Fermi level corresponds to the Fermi level of bulk graphite, that is, the original Fermi level of the bulk graphite is lower by about 2.5 eV relative to the Fermi level of monolayer graphite on the TiC(111) surface, and the originally unoccupied π^* band of the bulk graphite is partially occupied.

In contrast to the occupied bands, the unoccupied π^* bands are drastically deformed. The most striking feature is that the bands with strong π character are

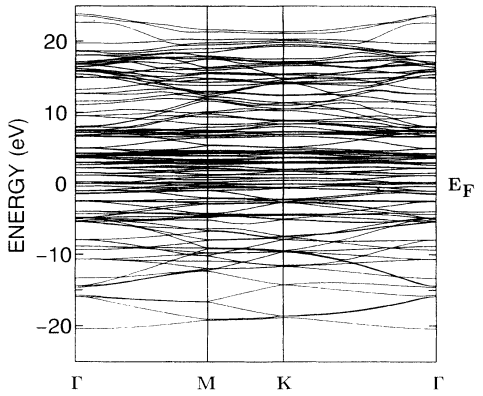

FIG. 2. Calculated band structure of monolayer graphite on TiC(111) for model A, when the graphite-substrate distance is 2.16 Å. The origin of the energy is chosen as the Fermi energy.

scarcely seen in the energy region from 0 to 5 eV above the Fermi level. In this region, the π bands are strongly mixed with the $3d$ bands of Ti and distributed over many bands. This is evident from Figs. 3(b), 4, and 5. Figure 3(b) shows the bands for which the $3d$ component of the top-layer Ti is larger than 25%. The $3d$ bands of the Ti

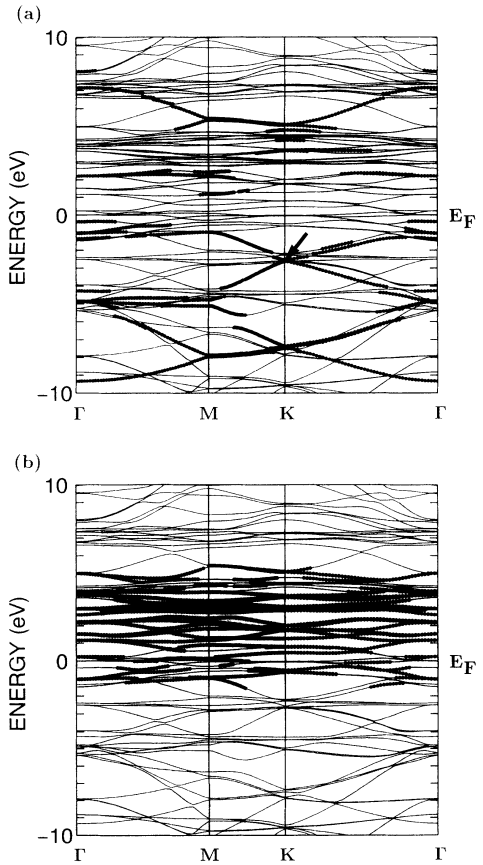

FIG. 3. Calculated (a) π band and (b) $3d$ band structure of monolayer graphite on TiC(111) for model A, when the graphite-substrate distance is 2.16 Å. Heavy lines indicate the bands whose (a) $2p_z$ component of the graphite layer and (b) $3d$ component of the first-layer Ti are larger than 25%. The arrow indicates the point corresponding to the Fermi level of an isolated graphite monolayer.

layer are concentrated in the region from -1 to $+5$ eV. Figure 4 shows the $2p_z$ components of the graphite and the $3d$ component of the top-layer Ti in the total density of states. The occupied region of the partial density of states (PDOS) of the graphite shows a π band structure similar to that of bulk graphite. However, the unoccupied region is deformed by being mixed with the $3d$ bands of Ti. The feature of energy-dependent mixing is also seen in Fig. 5, which shows the LDOS in a plane containing the C atoms of graphite and the Ti atoms perpendicular to the surface. The mixing of the wave functions between the graphite layer and the substrate is weak for the occupied states and stronger for the unoccupied states near the Fermi level.

When the graphite-substrate distance is as long as the interlayer spacing of bulk graphite, the electronic structure of the graphite layer becomes almost the same as that of bulk graphite. Figure 6 shows the band structures for the case with the distance 3.42 Å. When the graphite-substrate distance is 3.42 Å, the mixing of the π bands and the $3d$ bands is much reduced, and the unoccupied π bands are well distinguished. As the distance increases, the original Fermi level of the bulk graphite rises toward the Fermi level of the monolayer graphite on the

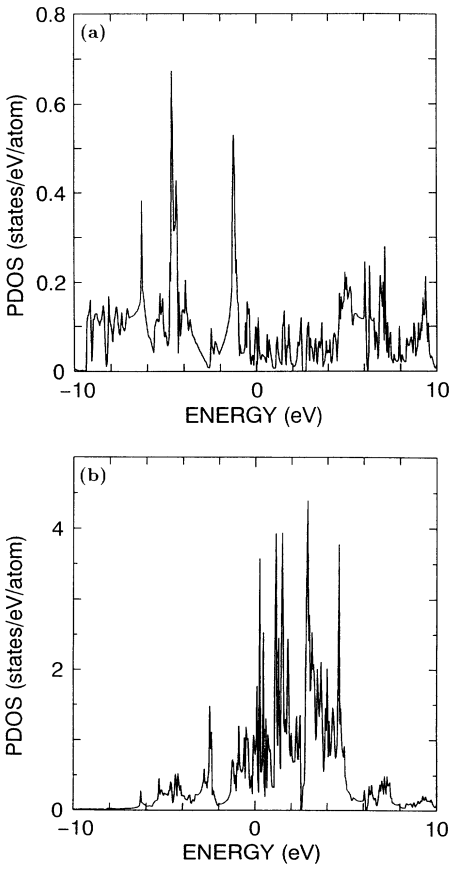

FIG. 4. Calculated PDOS of monolayer graphite on TiC(111) for model A, when the graphite-substrate distance is 2.16 Å: (a) π component of the graphite layer and (b) $3d$ component of the top-layer Ti of the TiC(111) surface. The origin of the energy is chosen as the Fermi level.

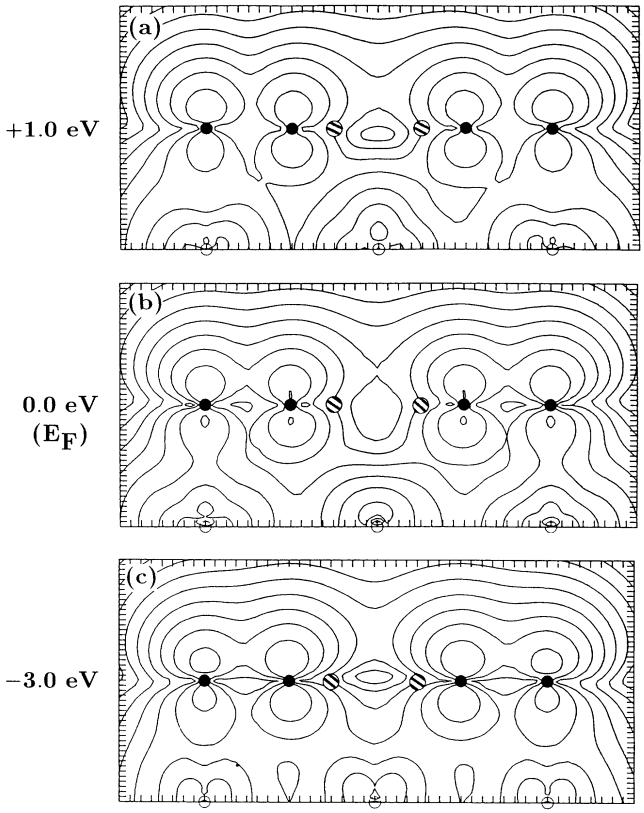

FIG. 5. Calculated LDOS in a plane normal to the surface of monolayer graphite on TiC(111) for model A, when the graphite-substrate distance is 2.16 Å. The energy is selected to be (a) 1.0 (b) 0.0, and (c) -3.0 eV. The closed and open circles indicate the positions of the C atoms of the graphite layer and the top-layer Ti atoms of the TiC(111) surface, respectively. These are situated on the cut plane. The hatched circles indicate the position of the C atoms of the graphite layer that are situated out of the cut plane.

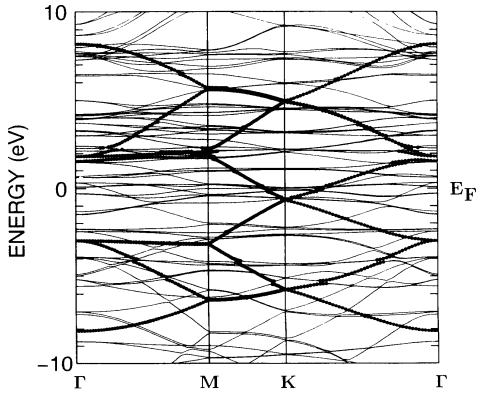

FIG. 6. Calculated π band structure of monolayer graphite on TiC(111) for model A, when the graphite-substrate distance is 3.42 Å. Heavy lines indicate the bands for which the $2p_z$ component of the graphite layer is larger than 25%.

substrate. The distance dependence of the energy shift of the π bands relative to the Ti d bands shows that the lowering of the π bands is not caused by the expansion of the graphite lattice by 6%, and that orbital hybridization between the graphite layer and the substrate is important in this system. In contrast to the π band structure, the $3d$ band structure of the Ti layer is not much changed.

To determine the graphite-substrate distance, the calculated band structure is compared with an experimental dispersion obtained from ARUPS.[12] Figure 7 shows the band structure projected from the 2×2 to the 1×1 Brillouin zone of bulk graphite for the case where the graphite-substrate distance is 2.16 Å. Agreement between the theory and the experiment is fairly good. The important point is that the K point of the experiment, which corresponds to the original Fermi level of bulk graphite, is also located at about 3 eV below the Fermi level of monolayer graphite on the TiC(111) surface. This result shows that the graphite-substrate distance is not so large as 3.42 Å, but is fairly small at 2.16 Å.

The fact that the original Fermi level of the bulk graphite is below the Fermi level in monolayer graphite on a substrate seems to support the charge-transfer mechanism from the substrate to the graphite layer proposed for explaining the softening in the phonon structure.[4] This is, however, not true. Table I shows the electronic charge at each atomic site estimated by Mulliken population analysis.[22] In the TiC layers, electrons are transferred from the Ti atom to the C atom. The degree of electronic polarization in the outer layers is small compared to that in the inner layers due to depolarization.[25–27] In contrast, no charge transfer between the graphite and the substrate occurs in spite of the short distance between the C atom in the graphite layer and the Ti atom. The graphite layer remains neutral. This result is reasonable, because the difference in work function between the bulk graphite surface and the TiC(111) surface is as small as 0.1 eV.[12]

These features of monolayer graphite on TiC(111) are different from those of the many donor GIC's.[10] In the GIC's, intercalants act merely as donors or acceptors of electrons, and orbital mixing between the graphite and the intercalants can be neglected. In such a case, the rigid-band model is valid, in which the Fermi level shifts according to the amount of charge transfer.

Unlike the case of the GIC's, charge transfer between the graphite layer and the substrate does not occur in monolayer graphite on the TiC(111) surface. Orbital mixing between the graphite and the substrate results in lowering of the π bands. The mechanism of the lowering is a change of electronic occupation in the graphite layer from occupied σ and π states to unoccupied π^* states, which can be explained as follows.

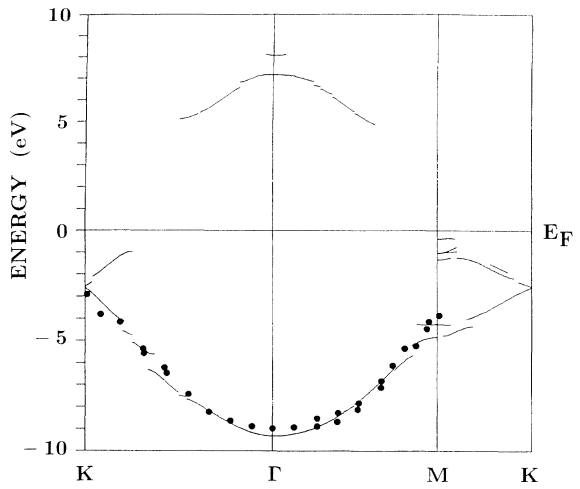

FIG. 7. Comparison of the calculated π band structure of monolayer graphite on TiC(111) with experimental data. The solid lines indicate the calculated bands, which are obtained from the data shown in Fig. 3(a) projected into the 1×1 Brillouin zone of bulk graphite. Closed circles show the experimental dispersions obtained from ARUPS data by Nagashima *et al.*[12]

By a simple tight-binding calculation, the amount of change in electronic charge due to orbital mixing between the graphite layer and the substrate is estimated as

$$\Delta n_\sigma = -\sum_{\sigma,S}(1-\tilde{\lambda}_S)\left[\frac{t_{\sigma S}}{\varepsilon_S-\varepsilon_\sigma}\right]^2, \tag{3}$$

$$\Delta n_\pi = -\sum_{\pi,S}(1-\tilde{\lambda}_S)\left[\frac{t_{\pi S}}{\varepsilon_S-\varepsilon_\pi}\right]^2, \tag{4}$$

$$\Delta n_{\pi^*} = \sum_{\pi^*,S}\tilde{\lambda}_S\left[\frac{t_{\pi^* S}}{\varepsilon_S-\varepsilon_{\pi^*}}\right]^2 + \sum_{\pi^*}\tilde{\lambda}_{\pi^*}, \tag{5}$$

where σ, π, π^*, and S are labels denoting the occupied σ state, the occupied π state, the unoccupied π^* state of graphite, and the substrate state, respectively. In the above, ε_σ, ε_π, ε_{π^*}, and ε_S are the energies of each state, and $t_{\sigma S}$, $t_{\pi S}$, and $t_{\pi^* S}$ are graphite-substrate transfer en-

TABLE I. Electron numbers of atoms in each layer for models A and B estimated by Mulliken population analysis. The surface-substrate distance d is 2.16 and 3.42 Å, respectively. ΔQ denotes the difference of the electron number from neutral.

	Model A $d=2.16$ Å		Model B $d=2.16$ Å		Model A $d=3.42$ Å	
	Q	ΔQ	Q	ΔQ	Q	ΔQ
C (graphite layer)	6.00	±0.00	6.00	±0.00	6.00	±0.00
Ti (first layer)	21.88	−0.12	21.89	−0.11	21.86	−0.14
C (second layer)	6.18	+0.18	6.19	+0.19	6.20	+0.20
Ti (third layer)	21.88	−0.12	21.88	−0.12	21.90	−0.10
C (fourth layer)	6.04	+0.04	6.04	+0.04	6.03	+0.03

ergies. The quantities λ_S and λ_{π^*} represent the occupation of the substrate state and the graphite π^* state, respectively. The values $\lambda=0$ and $\lambda=1$ correspond to the unoccupied and the fully occupied state, respectively. The quantities with a tilde are those changed from the original values by the graphite-substrate transfer. The sum is taken of all the σ, π, π^*, and substrate states.

Equations (3) and (4) express the reduction of electronic occupation in the occupied σ and π states of the graphite layer due to orbital mixing with unoccupied substrate states. On the other hand, the first term of the right-hand side in Eq. (5) expresses the increase of electronic occupation in the unoccupied π^* states due to mixing with the occupied substrate states. In the case of the TiC(111) substrate, the substrate band near the Fermi level is the Ti $3d$ band, which is metallic and partially occupied as shown in Fig. 3(b). This causes a reduction of electronic charge in the occupied σ and π bands, and an increase in occupation in the unoccupied π^* band. Furthermore, the $3d$ bands of the substrate are concentrated in the higher-energy region above the Fermi level. This favors a lowering of the orbital energy in the lower-energy region of the π^* band as

$$\tilde{\varepsilon}_{\pi^*}=\varepsilon_{\pi^*}-\sum_S \frac{t^2_{\pi^* S}}{\varepsilon_S-\varepsilon_{\pi^*}} . \tag{6}$$

However, since the bandwidth of graphite is wider than that of the substrate $3d$ band, the lowering of the substrate orbital energy due to mixing with the higher-energy part of the graphite band is compensated for by the increase due to mixing with the lower-energy part of the graphite band. The orbital energy of the substrate does not change much. Therefore, the lower-energy part of the unoccupied π^* band is lowered under the original Fermi level, and the electronic charge transfer from the occupied substrate bands to the unoccupied π^* band. The second term of the right-hand side in Eq. (5) expresses the increase of occupation in the π^* band due to this direct charge transfer. These features are seen in the orbital components of the calculated Mulliken charge shown in Table II. Compared with bulk graphite, the occupancy in the σ states is reduced, and that of the π states increased in the monolayer graphite. The reduction of electronic charge in the occupied σ and π bands is compensated for by the increase in the unoccupied π^* band, and the graphite remains neutral. This is the mechanism of the lowering of the energy of the π band without a significant charge transfer from the substrate.

The reduction of the energy in the system due to the graphite-substrate mixing is estimated as

$$\Delta E=-\sum_{\sigma,S}(1-\lambda_S)\frac{(t_{\sigma S})^2}{\varepsilon_S-\varepsilon_\sigma}-\sum_{\pi,S}(1-\lambda_S)\frac{(t_{\pi S})^2}{\varepsilon_S-\varepsilon_\pi}$$
$$-\sum_{\pi^*,S}\lambda_S\frac{(t_{\pi^* S})^2}{\varepsilon_{\pi^*}-\varepsilon_S}+\sum_{\pi^*}(\tilde{\varepsilon}_{\pi^*}-\tilde{\varepsilon}_F)\Delta\lambda_{\pi^*}$$
$$+\sum_S(\tilde{\varepsilon}_S-\tilde{\varepsilon}_F)\Delta\lambda_S , \tag{7}$$

where $\Delta\lambda_{\pi^*}$ and $\Delta\lambda_S$ are the difference in electronic occupation of the π^* and the substrate states, respectively. The first three terms of the right-hand side in Eq. (7) express the stabilization due to orbital mixing between the

TABLE II. Orbital component of electron numbers in the graphite layer for models A and B estimated by Mulliken population analysis. The surface-substrate distance d is 2.16 Å for (a) and (b), and 3.42 Å for (c). Types of C atoms correspond to the numbers in Fig. 1. ΔQ denotes difference of the electron number from neutral. For comparison, the orbital component calculated for isolated monolayer graphite without the substrate is shown in (d).

	$2s$	$2p_\sigma$	$2p_\pi$	σ $(=2s+2p_\sigma)$	Total $(=2s+2p_\sigma+2p_\pi)$	(ΔQ)
			(a) Model A ($d=2.16$ Å)			
Type 1	1.18	1.81	1.01	2.99	3.99	(−0.01)
Type 2	1.14	1.75	1.13	2.89	4.02	(+0.02)
Average	1.17	1.79	1.04	2.96	4.00	(±0.00)
			(b) Model B ($d=2.16$ Å)			
Type 1	1.16	1.78	1.07	2.94	4.01	(+0.01)
Type 2	1.18	1.81	1.00	2.98	3.98	(−0.02)
Type 3	1.18	1.81	1.01	2.99	4.00	(±0.00)
Type 4	1.16	1.79	1.07	2.95	4.01	(+0.01)
Average	1.17	1.80	1.04	2.96	4.00	(±0.00)
			(c) Model A ($d=3.42$ Å)			
Type 1	1.19	1.81	1.00	3.00	4.01	(+0.01)
Type 2	1.19	1.81	1.00	2.99	4.00	(±0.00)
Average	1.19	1.81	1.00	3.00	4.00	(±0.00)
			(d) Isolated monolayer graphite			
Graphite	1.19	1.82	1.00	3.00	4.00	(±0.00)

graphite and the substrate. The fourth and fifth terms express the stabilization due to charge transfer from the substrate to the graphite. The latter terms contribute to the stabilization, because $\Delta\lambda_{\pi^*}>0$ and $\tilde{\varepsilon}_{\pi^*}-\tilde{\varepsilon}_F<0$ for the graphite, and $\Delta\lambda_S<0$ and $\tilde{\varepsilon}_S-\tilde{\varepsilon}_F>0$ for the substrate. Since the energy difference $\varepsilon_{\pi^*}-\varepsilon_S$ is smaller and the transfer energy t_{π^*S} is larger than the other terms in the case of monolayer graphite on the TiC(111) surface, the third term is the main contribution to stabilization by orbital mixing.

This mechanism suggests anomalous expansion of the C-C bond length in monolayer graphite compared to GIC's. In the GIC's, the mechanism of expansion of the bond length is the π-bond weakening due to charge transfer into the unoccupied π^* band.[11] In the present case, the electronic occupation in the σ states decreases due to coupling with the substrate. The influence of the σ bond on the bond-length expansion would be much stronger than that of the π bond. This is similar to the donation and back-donation mechanism of CO chemisorption on transition-metal surfaces.[28,29]

The stable structure is determined by the balance between the energy gained by the graphite-substrate mixing and that lost by the weakening of the C-C bond in the graphite layer caused by the graphite-substrate mixing. In the case of monolayer graphite on the TiC(100) surface, the surface bands of the TiC(100) substrate near the Fermi level are fully unoccupied.[25] The energy gain by the third, fourth, and fifth terms in Eq. (7) is lost. This may explain the fact that the phonon structure of monolayer graphite on a TiC(100) surface does not show softening.[4,5]

It may be supposed that, since the bonding between the graphite layer and the substrate is essential, the results obtained may depend on the lateral position of the graphite layer relative to the substrate. A band calculation for model B shown in Fig. 1(b) was also performed. Figure 8 shows the calculated band structure for the case where the graphite-substrate distance is 2.16 Å. Contrary to the above expectation, the band structure obtained is almost the same as that of model A shown in Fig. 3(a). As shown in Table I, the calculated charges also do not differ from those of model A within the computational accuracy. The reason for these results can be shown as follows.

Not all the C atoms in the graphite layer of both model A and model B are equivalent. For model A, there are two kind of C atoms. One is situated just above the substrate Ti atom, and the other is above the point midway between two Ti atoms. The former is the position where the interaction with the Ti atom is strongest, and the latter is the weakest position. In contrast, the C atoms in model B are positioned where the strength of the interaction with the Ti atom is midway between those of the two kind of atoms in model A. On average over the atoms, the strength of the interaction with the substrate is roughly equal between these models, and the overall features of the band structure are not much different. This is also seen in the calculated Mulliken charges, as shown in Table II, where the charges are site dependent and are different in the two models, but the averaged values over the unit cell do not differ. The appearance of this averaging effect even with such a relatively small unit cell is ascribed to the lattice mismatch between the overlayer and the substrate. The small difference of the calculated band dispersion between the different graphite-substrate geometries means that broadening of the AR-UPS peaks of graphite caused by the incommensurate substrate is small, and that distinct band dispersions can be observed even in the present system with its strong substrate-overlayer interaction.

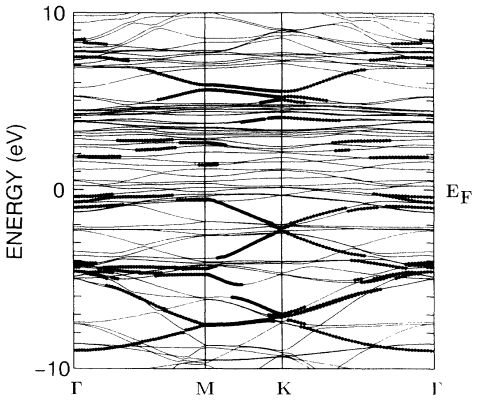

FIG. 8. Calculated π band structure of monolayer graphite on TiC(111) for model B, when the graphite-substrate distance is 2.16 Å. The heavy lines indicate the bands for which the $2p_z$ component of the graphite layer is larger than 25%.

B. STM images

Figure 9 shows calculated STM images of monolayer graphite on a TiC(111) surface. The calculation is performed for model A in Fig. 1 with the graphite-substrate distance 2.16 Å. The LDOS is calculated at points 5.3 Å above the graphite layer. The tunneling current is calculated for the sample bias voltage (a) +0.5 and (b) −0.5 V. The calculated STM image of monolayer graphite on the TiC(111) surface shows a triangular pattern, which is different from the honeycomb atomic structure of graphite. This is similar to the STM image of pristine graphite. However, the peak regions of the tunneling current form the 2×2 structure of the original graphite unit cell. The period of the pattern is 5.3 Å. The calculated STM image reproduces well the features of experimental STM images, which show the triangular pattern with a period of about 5 Å.[14]

An interesting feature of this image is that the peaks are located not at the C atomic sites but at the hollow sites surrounded by six C atoms. The individual atomic image of the C atoms is not seen, which is similar to the STM image of the benzene molecule.[30–33] The features of the STM image depend on the height of the viewpoint from the surface. When this height is taken as 2.6 Å, the intensity at the hollow site decreases and the region with large current intensity is located at the C atomic sites. The STM image comes to resemble a doughnut.

The tunneling current takes a minimum value at the remaining two C sites. Hereinafter, these two C sites are called the minor site, and the other bright sites are called the major site. The site dependence of the tunneling

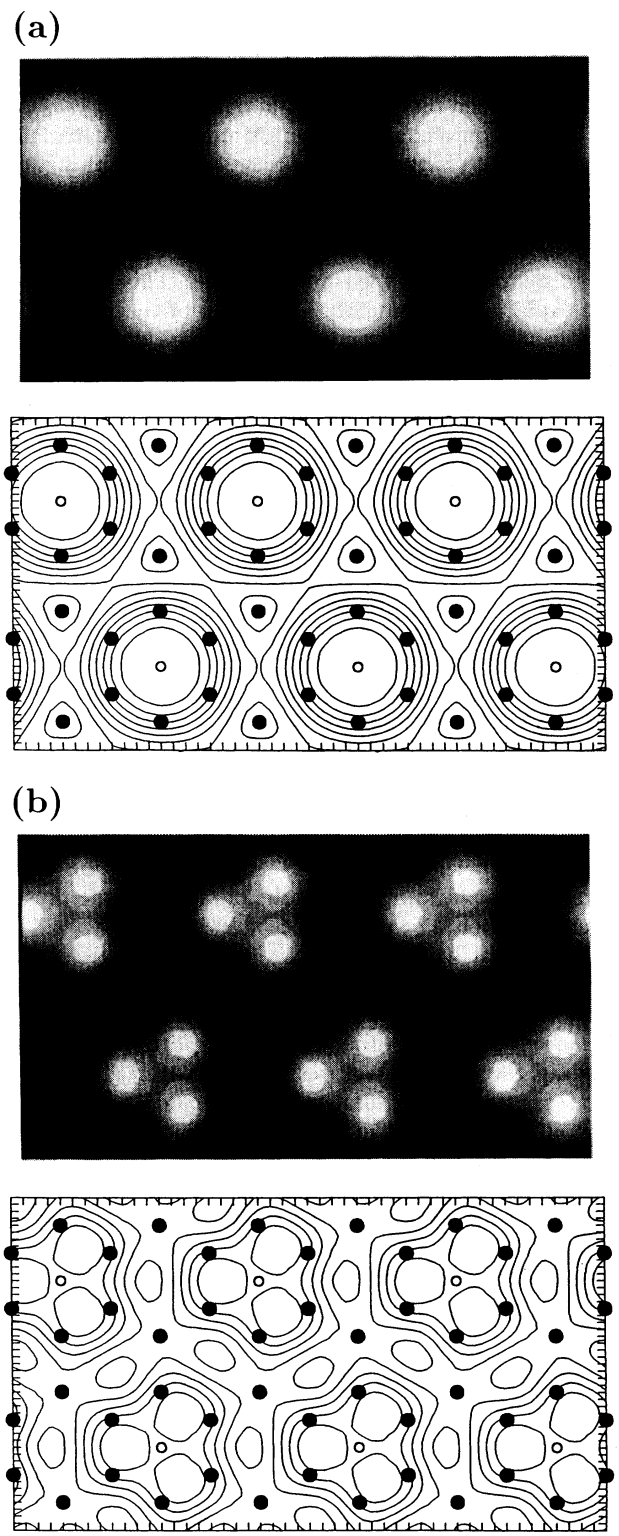

FIG. 9. Calculated STM images of monolayer graphite on TiC(111) for model A, when the graphite-substrate distance is 2.16 Å. The tunneling current is calculated for the sample bias voltage (a) +0.5 and (b) −0.5 V. The upper and lower parts of the figures are a gray-scale image and a contour map, respectively. Spacing of the contours is $\frac{1}{10}$ of the current maximum. Closed and open circles indicate the positions of the C atoms of the graphite layer and the Ti atoms of the first substrate layer. The images show a triangular-lattice pattern.

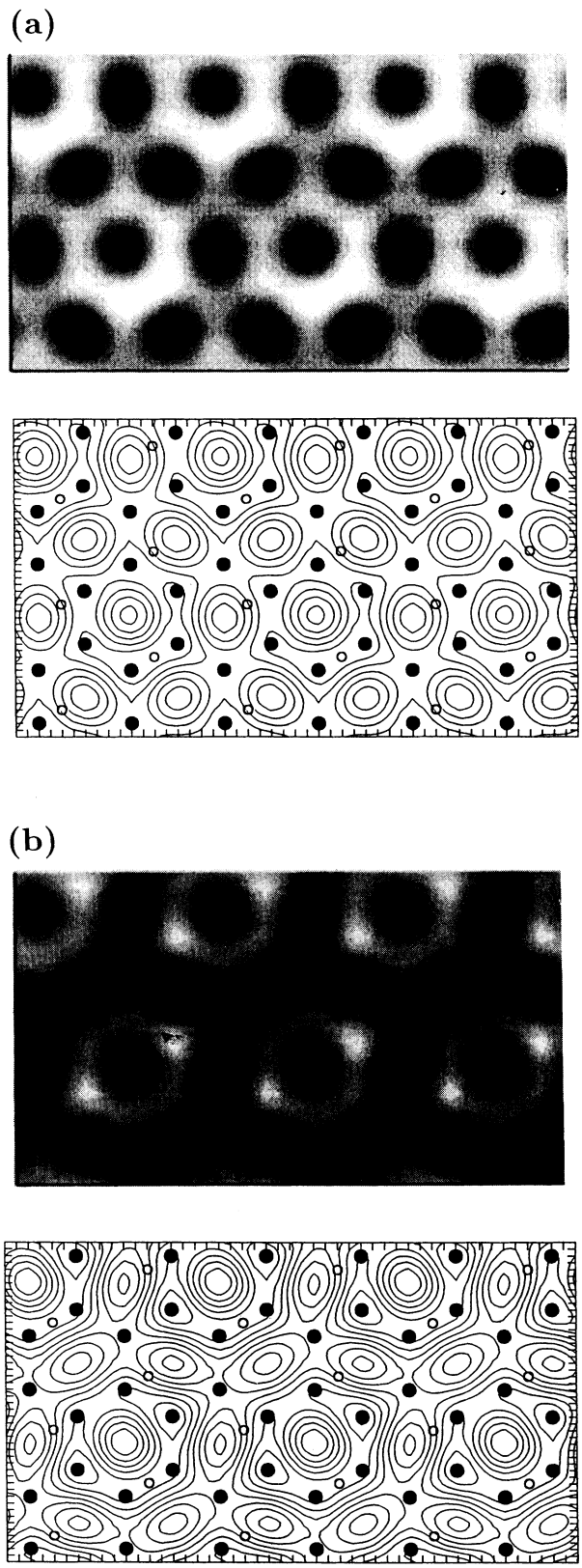

FIG. 10. Calculated STM image of monolayer graphite on TiC(111) for model B, when the graphite-substrate distance is 2.16 Å. The tunneling current is calculated for the sample bias voltage (a) +0.5 and (b) −0.5 V. Other conditions are the same as in Fig. 9. The image changes from a honeycomb-lattice to a triangular-lattice structure depending on the bias voltage.

current reflects the site dependence of the interaction strength with the substrate. The Ti atoms of the substrate are located just below the minor sites, but not below the major sites. Orbital hybridization between the C atoms and the Ti atoms forms bonding and antibonding orbitals, and tends to reduce the number of states near the Fermi level. Since the interaction of the minor sites with the substrate is stronger than that of the major sites, the tunneling current at the minor sites is reduced. These features do not show a significant energy dependence within about ± 1 eV around the Fermi level, as shown in Fig. 9(b).

In contrast, the STM image for model B shows the energy dependence depicted in Fig. 10. The STM image of the unoccupied states shows a honeycomb structure, which is the lattice image of graphite, and the image of the occupied states shows a 2×2 structure similar to that of model A. However, the regions of the weakest tunneling current in model B are located not above the C atomic sites but above the hollow sites. Comparing models A and B, it is reasonable that the 2×2 structure tends to appear for model A, because the site difference of the interaction between the graphite C atoms and the substrate is larger in model A. When the bias voltage is gradually changed from -0.5 to $+0.5$ V, the STM image of the occupied states deforms continuously to that of the unoccupied states.

The experimental STM images of monolayer graphite on TiC(111) depend on the polarity of the applied bias voltage.[14] The image of the unoccupied states shows only a triangular structure with a period of about 5 Å. In the image of the occupied states, a modulation with a period as long as 21 Å is added to the triangular structure, and the STM image shows a moiré pattern. The calculated STM images of the unoccupied states show a 2×2 triangle pattern for both models A and B, and the images of the occupied states change depending on the model. This may indirectly explain the fact that the moiré pattern is seen in the occupied state and not in the unoccupied state, but it is not so clear in the present small unit cell. To discuss the moiré pattern explicitly, an electronic-structure calculation with a large unit cell is needed. At present, it is difficult to perform a first-principles band calculation with such a large unit cell. Instead, a tight-binding calculation would be effective.

IV. CONCLUSIONS

In this paper, the electronic structure of monolayer graphite on a TiC(111) surface has been investigated by first-principles band calculations. The occupied π bands of the graphite layer are similar to those of bulk graphite. The original Fermi level in bulk graphite is lower by about 2.5 eV than the Fermi level of monolayer graphite on TiC(111). The unoccupied π^* bands are drastically changed from those of bulk graphite, and are partially occupied. This has been explained by hybridization between the π orbitals of the graphite and the $3d$ orbitals of the substrate Ti layer. The calculated band dispersion well reproduced the experimental data.

The electronic charge at each site has been calculated, and shows no charge transfer between the graphite layer and the substrate. The lowering of the π bands has been explained by the change of electronic occupation from the occupied σ and π states to the unoccupied π^* states, due to hybridization with the substrate. This mechanism may explain the anomalous expansion of the lattice constant in monolayer graphite and substrate dependence of the phonon structure. The results obtained are not changed by a lateral shift of the graphite layer over the substrate. This fact has been explained by the averaging effect in the lattice-mismatched system.

The STM image has been calculated with the results of the band calculations. The calculated images show a 2×2 superstructure of the graphite lattice, which explains the superstructure with the shorter period observed in the experiment. The calculated STM images depend on the lateral position of the graphite layer relative to the substrate, which indirectly explains the energy dependence of the observed moiré pattern. To discuss the moiré pattern explicitly, an electronic-structure calculation with a large unit cell is desirable, and will be presented in future.

In the present study, the distance between the graphite layer and the substrate has been determined not by a first-principles total-energy calculation but by comparison with experiment. A total-energy calculation is important for confirming the results obtained in the present paper, and should be performed in future.

The present work may be extended to investigation of the electronic structure of monolayer graphite on other metal substrates such as TiC(110), TaC(111), and Pt(111). The investigation of other cases is important for understanding the general features of monolayer graphite on metal substrates. A first-principles calculation of the phonon structure for monolayer graphite on substrates would be interesting for investigating the softening mechanism of the phonon dispersion observed in experiment. The discussion of the moiré pattern in STM should be extended to other surfaces and layered materials such as $MoSe_2/MoS_2$, where the moiré pattern is observed even when ten overlayers are accumulated.[34,35]

ACKNOWLEDGMENTS

The authors thank C. Ohshima, T. Aizawa, H. Ito, and A. Nagashima for valuable discussions. Numerical calculations are performed by the HITAC S-820 computer system at the Computer Center of the University of Tokyo and the Institute for Molecular Science. This work is partially supported by a Grant-in-Aid from the Ministry of Education, Science and Culture, Japan.

[1]P. Hansma and J. Tersoff, J. Appl. Phys. **61**, R1 (1987).
[2]Sang-Il Park and C. F. Quate, Appl. Phys. Lett. **48**, 112 (1986).
[3]D. Tománek and S. G. Louie, Phys. Rev. B **37**, 8327 (1988).
[4]T. Aizawa, R. Souda, S. Otani, Y. Ishizawa, and C. Oshima, Phys. Rev. Lett. **64**, 768 (1990); Phys. Rev. B **42**, 11 469 (1990).
[5]T. Aizawa, R. Souda, Y. Ishizawa, H. Hirano, T. Yamada, and K. Tanaka, Surf. Sci. **237**, 194 (1990).
[6]T. Aizawa, Y. Hwang, W. Hayami, R. Souda, S. Otani, and Y. Ishizawa, Surf. Sci. **260**, 311 (1992).
[7]Y. Hwang, T. Aizawa, W. Hayami, S. Otani, Y. Ishizawa, and S. J. Park, Solid State Commun. **81**, 397 (1992).
[8]Y. Hwang, T. Aizawa, W. Hayami, S. Otani, and Y. Ishizawa, Surf. Sci. **271**, 299 (1992).
[9]K. Yamamoto, M. Fukushima, T. Osaka, and C. Oshima, Phys. Rev. B **45**, 11 358 (1992).
[10]M. S. Dresselhaus and G. Dresselhaus, Adv. Phys. **30**, 139 (1981).
[11]C. T. Chen, W. A. Kamitakahara, K. M. Ho, and P. C. Eklund, Phys. Rev. Lett. **58**, 1528 (1987).
[12]A. Nagashima, K. Nuka, H. Itoh, T. Ichnokawa, C. Oshima, and S. Otani, Surf. Sci. **291**, 93 (1993).
[13]A. Nagashima, K. Nuka, H. Itoh, T. Ichinokawa, C. Oshima, S. Otani, and Y. Ishizawa, Solid State Commun. **83**, 581 (1992).
[14]H. Itoh, T. Ichinose, C. Oshima, and T. Ichinokawa, Surf. Sci. **254**, L437 (1991).
[15]T. A. Land, T. Michely, R. J. Behm, J. C. Hemminger, and G. Comsa, Surf. Sci. **264**, 261 (1992); J. Chem. Phys. **97**, 6774 (1992).
[16]R. Rosei, M. De Crescenzi, F. Sette, C. Quaresima, A. Savoia, and P. Perfetti, Phys. Rev. B **28**, 1161 (1983).
[17]J. C. Slater, T. M. Wilson, and J. H. Wood, Phys. Rev. **179**, 29 (1969).
[18]R. Srinivasan and G. Lakshmi, Surf. Sci. **43**, 617 (1974).
[19]A. Zunger and A. J. Freeman, Phys. Rev. B **15**, 4716 (1977).
[20]P. Hohenberg and W. Kohn, Phys. Rev. **136**, B864 (1964).
[21]W. Kohn and L. J. Sham, Phys. Rev. **140**, A1133 (1965).
[22]R. S. Mulliken, J. Chem. Phys. **23**, 1841 (1955).
[23]J. Tersoff and D. R. Hamann, Phys. Rev. B **31**, 805 (1985).
[24]G. S. Painter and D. E. Ellis, Phys. Rev. B **1**, 4747 (1970).
[25]A. Fujimori, F. Minami, and N. Tsuda, Surf. Sci. **121**, 199 (1982).
[26]M. Tsukada and T. Hoshino, J. Phys. Soc. Jpn. **51**, 2562 (1982).
[27]T. Hoshino and M. Tsukada, J. Magn. Magn. Mater. **31-34**, 901 (1983).
[28]G. Blyholder, J. Phys. Chem. **68**, 2772 (1964).
[29]G. Doyen and G. Ertl, Surf. Sci. **43**, 197 (1974).
[30]H. Ohtani, R. J. Wilson, S. Chiang, and C. M. Mate, Phys. Rev. Lett. **60**, 2398 (1988).
[31]S. Ohnishi and M. Tsukada, Solid State Commun. **71**, 391 (1989).
[32]A. J. Fisher and P. E. Blöchl, Phys. Rev. Lett. **70**, 3263 (1993).
[33]M. Tsukada, T. Schimizu, S. Watanabe, N. Isshiki, and K. Kobayashi, Jpn. J. Appl. Phys. **32**, 1352 (1993).
[34]B. A. Parkinson, F. S. Ohuchi, K. Ueno, and A. Koma, Appl. Phys. Lett. **58**, 472 (1991).
[35]T. Mori, K. Saiki, and A. Koma, Jpn. J. Appl. Phys. **31**, L1370 (1992).

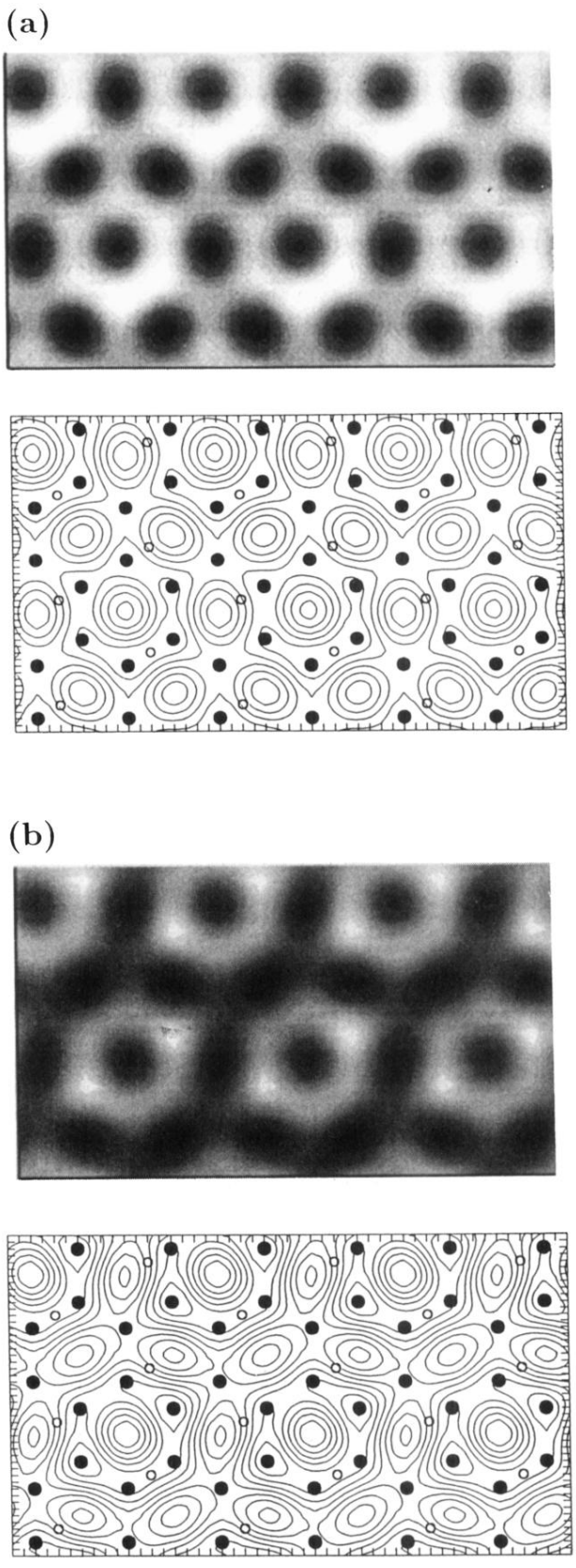

FIG. 10. Calculated STM image of monolayer graphite on TiC(111) for model B, when the graphite-substrate distance is 2.16 Å. The tunneling current is calculated for the sample bias voltage (a) $+0.5$ and (b) -0.5 V. Other conditions are the same as in Fig. 9. The image changes from a honeycomb-lattice to a triangular-lattice structure depending on the bias voltage.

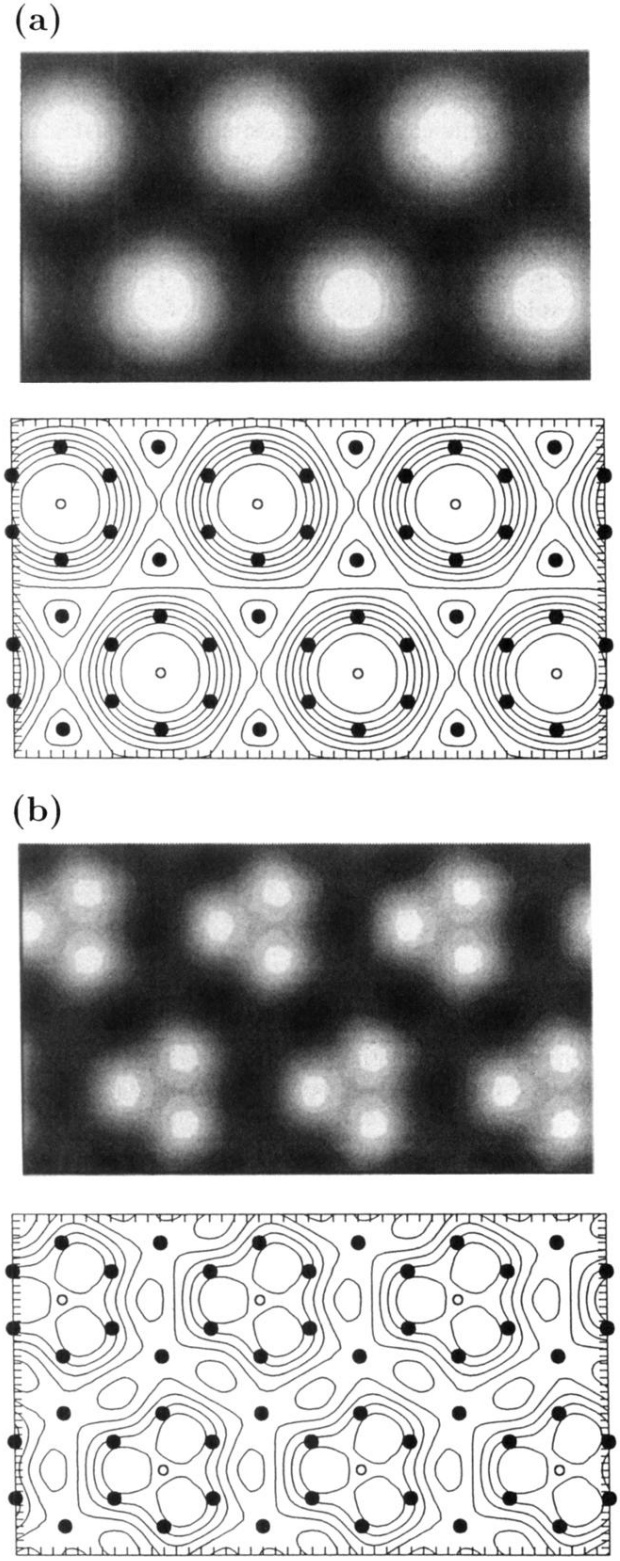

FIG. 9. Calculated STM images of monolayer graphite on TiC(111) for model A, when the graphite-substrate distance is 2.16 Å. The tunneling current is calculated for the sample bias voltage (a) $+0.5$ and (b) -0.5 V. The upper and lower parts of the figures are a gray-scale image and a contour map, respectively. Spacing of the contours is $\frac{1}{10}$ of the current maximum. Closed and open circles indicate the positions of the C atoms of the graphite layer and the Ti atoms of the first substrate layer. The images show a triangular-lattice pattern.